*Biomechanics and Modeling in Mechanobiology*

**Supplementary Material**

# Tissue Growth Constrained by Extracellular Matrix Drives Invagination during Optic Cup Morphogenesis

Alina Oltean[1], Jie Huang[2], David C. Beebe[2], Larry A. Taber[1]

[1]Department of Biomedical Engineering, Washington University, One Brookings Drive, Campus Box 1097, Saint Louis, MO 63130-4899, USA
E-mail: aoltean@go.wustl.edu, lat@wustl.edu
[2]Department of Ophthalmology and Visual Sciences, Washington University, Saint Louis, MO, 63130, USA

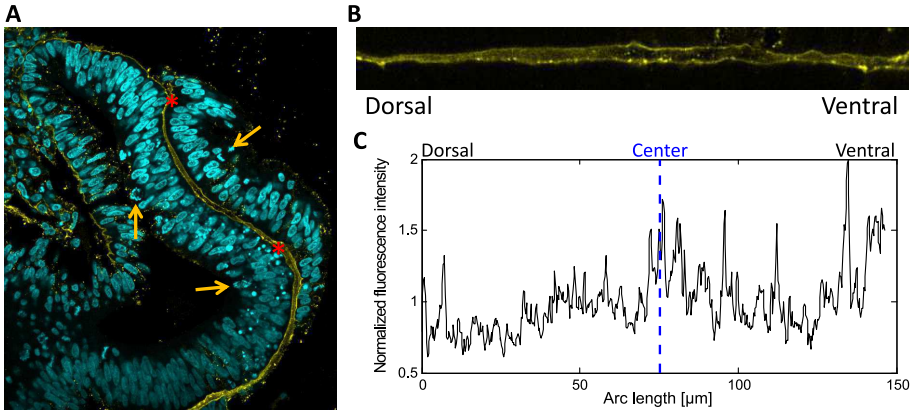


**Figure S1:** Matrix visualization in OV. (A) Confocal image of the invaginating OV and SE. Nuclei are cyan, fibronectin is yellow. Red asterisks (*) mark the start and end of the contact between the two cell layers. Orange arrows point to a few mitotic cells along the apical surfaces of the SE and OV during interkinetic nuclear migration. (B) The ECM from A was traced and the image straightened in ImageJ. (C) Fluorescence intensity was calculated and plotted by summing the columns along the dorsal half of the ECM arc length. Intensity and arc length were normalized for multiple samples to obtain the results shown in Fig. 9B.

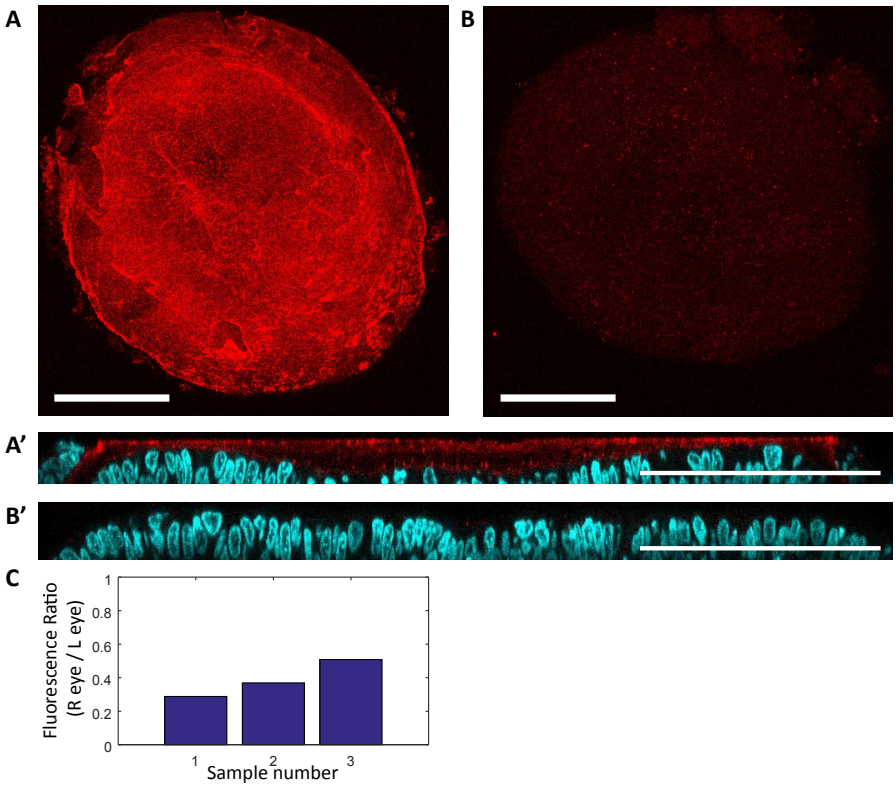


**Figure S2:** Effects of collagenase on matrix. (A) Confocal images of fibronectin staining (red) of two eyes from a representative embryo (Phase 3, HH14+). The basal surface of the OV was stained after SE removal (A, A') and after SE removal followed by local collagenase treatment (B, B') with the same confocal laser settings. (A, B) Stacks of 8 images of the ECM, combined in ImageJ according to maximum intensity of each image, show brighter staining in the eye without collagenase treatment. (A', B') Cross-sections of the ECM also show weaker fibronectin staining in the collagenase case (cyan = cell nuclei (dapi)). (C) Ratio of fibronectin intensity for three embryos (Phase 2–3). Ratio was computed as sum of intensity in B (collagenase treated) / sum of intensity in A (control). Collagenase reduced fibronectin staining in all embryos with an average fluorescence ratio of 0.39. Scale bars: 100μm.

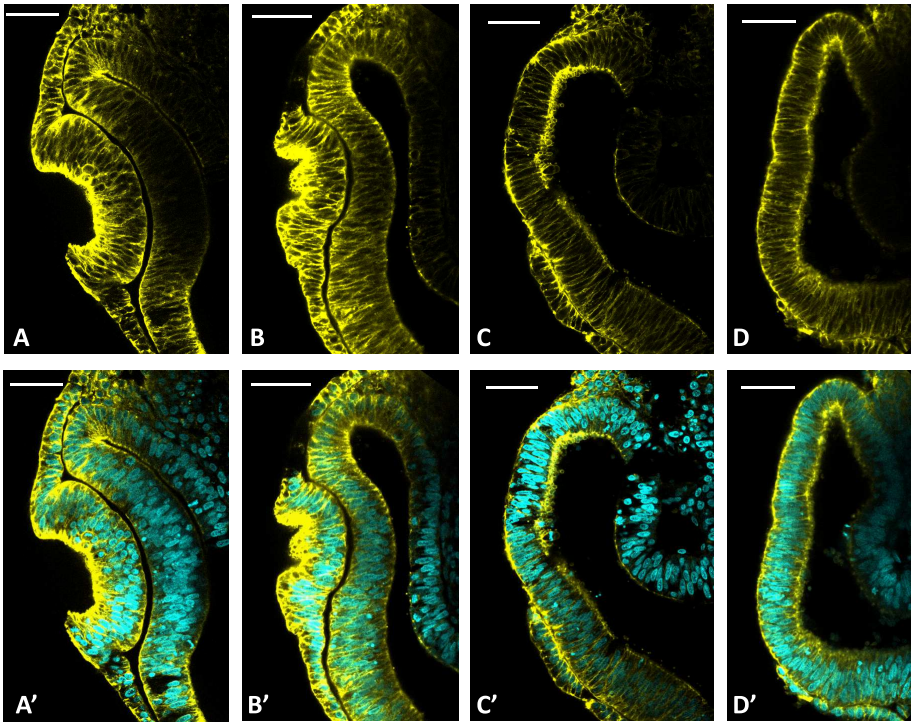


**Figure S3:** Effect of collagenase on F-actin. The right eyes of four chick embryos were stained for F-actin after SE removal and collagenase treatment (C, D, C', D'). Left eyes served as controls (A, B, A', B'). Eyes were stained, then sectioned in agarose and imaged with a confocal microscope. Four representative eyes are shown with actin in yellow (A–D, A'–D') and nuclei (DAPI) in cyan (A'–D'). Actin remained intact after SE removal and collagenase treatment. Scale bars: 50μm.

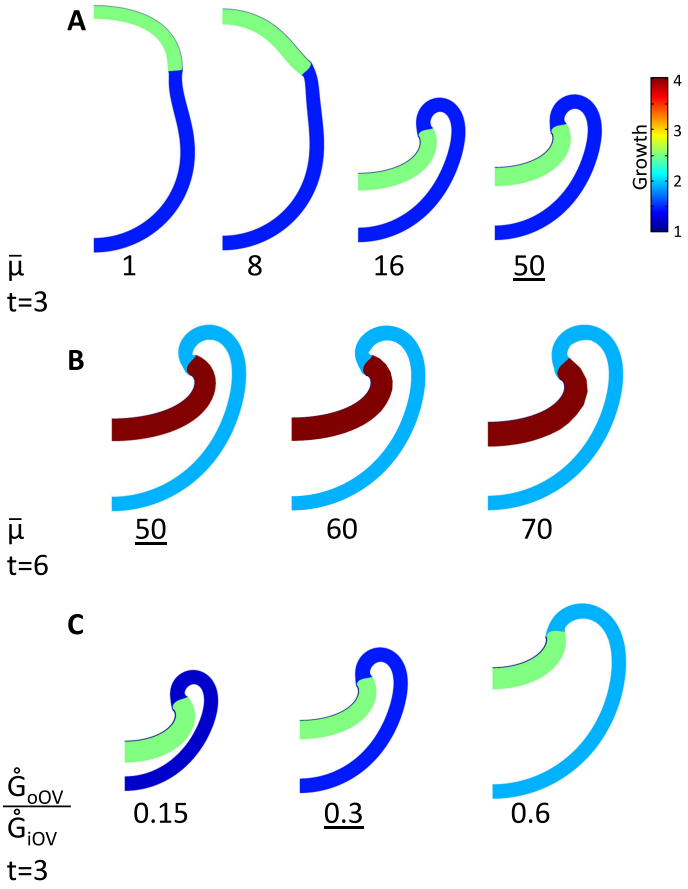


**Figure S4:** Effect of changing parameters in the uniform model (baseline model is underlined in each row). (A, B) Evagination occurs for low values of shear modulus ratio ($\bar{\mu} \leq 8$), while higher values lead to invagination and greater placode thickening. (C) Increasing the growth rate of the oOV had little effect on placode morphology but increased the distance between the iOV and oOV. Color bar shows values for $G$.

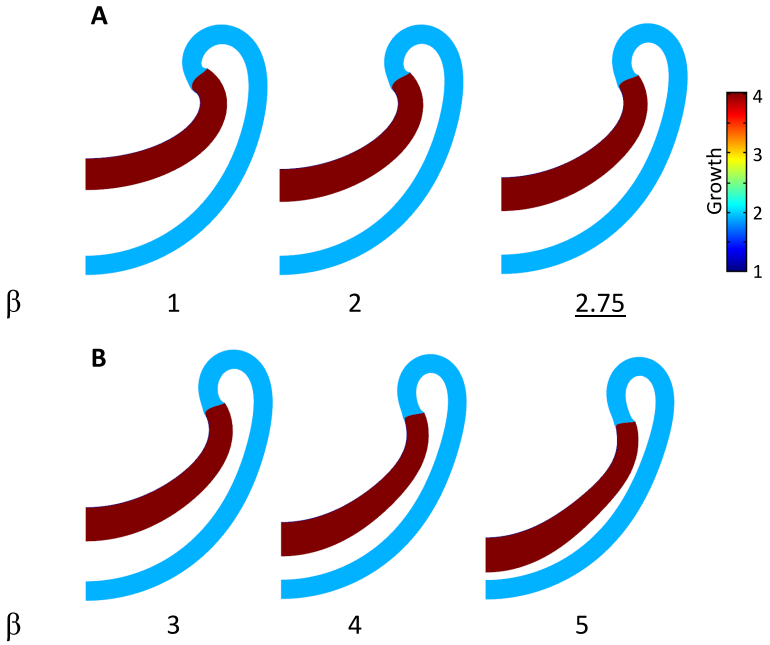


**Figure S5:** Effect of changing stiffness gradient parameter $\beta$ (see Eq. (6)) in OV model while preserving the average shear modulus ratio ($\bar{\mu} = 50$). Baseline stiffness gradient model is underlined. (A) Lower values of $\beta$ decrease the gradient in stiffness across the ECM and produce similar morphology as the uniform model. (B) Increasing $\beta$ leads to a lower shear modulus near the edge of the iOV and less constraint on iOV expansion. For this reason, large values of $\beta$ increase the invagination depth to levels considerably greater than those measured experimentally. Color bar shows values for growth ($G$).

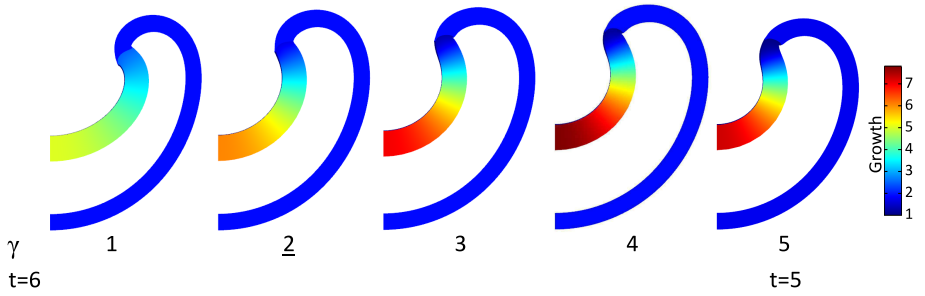


**Figure S6:** Effect of changing growth gradient parameter $\gamma$ (see Eq. (7)) in stiffness gradient model while preserving average iOV growth rate ($\mathring{G} = 0.5$). The baseline growth gradient model is underlined. As $\gamma$ increases, the growth gradient increases. Increasing $\gamma$ creates less realistic curvature in the iOV. Color bar shows values for growth ($G$). Models are shown at $t = 6$ except for $\gamma = 5$ due to convergence issues near the edge of the iOV.

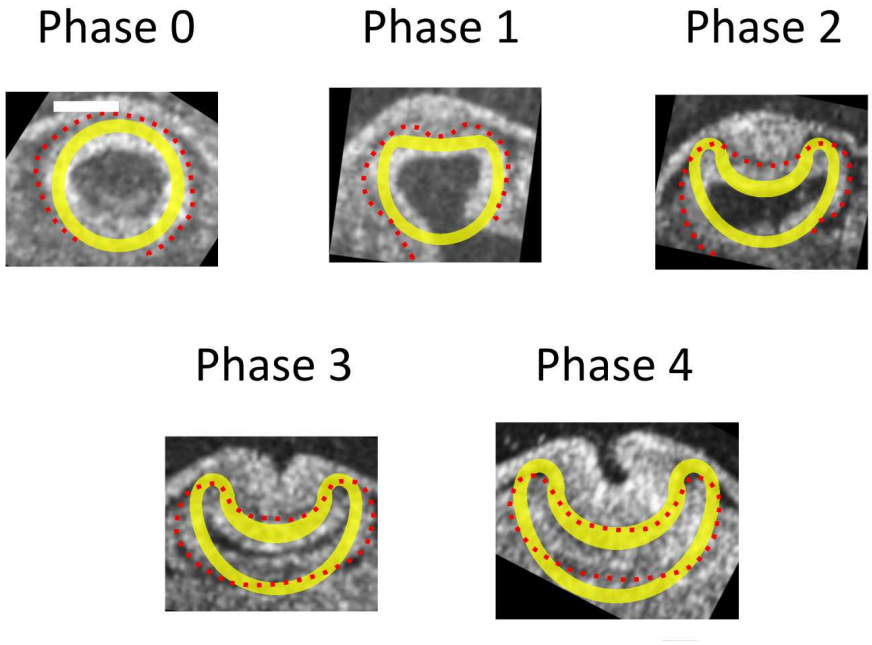


**Figure S7:** Overlay of chick OCT images at different stages and corresponding time points in the stiffness gradient model (yellow). Chick OVs (outlined in dashed red lines) are shown in the plane orthogonal to the optic stalk for greater symmetry. Model images were each scaled for the respective OCT image. Scale bar: 100µm.

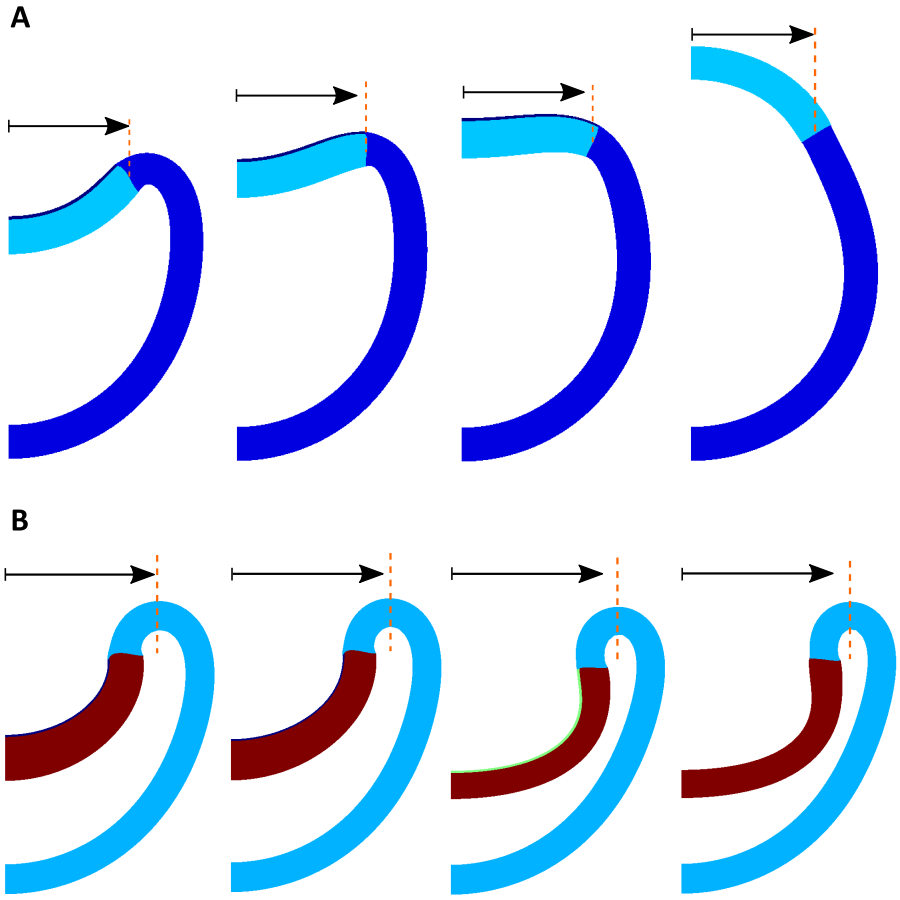


**Figure S8:** Intermediate steps for matrix degradation simulations. (A) Model evaginates (pops out) at Phase 2 (see Fig. 10A,A'). As ECM degrades, bending stresses at the edge of the invagination invert the iOV. Since the iOV has grown slightly larger than the opening created by the invagination, the iOV pushes the oOV outwards as it passes through the opening. To aid visualization, all arrows are the same length in each row and represent distance from the center of the OV to the edge of the invaginating region before degradation begins (left image). (B) Model remains invaginated at Phase 3 (see Fig. 10B, B'). The iOV has grown too large to overcome the constraint of the oOV as it tries to pass through the opening.